Supplementary data

Room temperature curing sustainable hybrid cross-linked coating enables efficient dynamic icephobicity of unmanned aerial vehicles

Xiangzhao Wang[a], Guiping Lin[a,b,], Zichen Zhang[a,]*, Kuiyuan Ma[a], and Jun Zhang[b]*

[a]Hangzhou International Innovation Institute, Beihang University, Hangzhou 311115 P. R. China

[b]School of Aeronautic Science and Engineering, Beihang University, Beijing 100191 P. R. China

*Corresponding author.

E-mail adress: zichenzhang437@buaa.edu.cn (Z. Zhang); gplin@buaa.edu.cn (G. Lin)

Experimental Section

Materials

Vanillin (VAN), tyramine (TA), tetrabutylammonium bromide (TBAB), and epichlorohydrin (ECH) were purchased from Shanghai Aladdin Reagent Co., Ltd. N. N-dimethylformamide (DMF), sodium hydroxide (NaOH), tetrahydrofuran (THF), ethyl acetate, anhydrous sodium sulfate, and hydrochloric acid were purchased from Shanghai Macklin Biochemical Co., Ltd. in China. Nano silica was purchased from Shandong Yousuo Chemical Technology Co., Ltd. Dimethyl silicone oil (10 CS) purchased from Dow Corning Co., Ltd. The superhydrophobic coating (SHC) was purchased from Dongguan Jinna New Materials Co., Ltd. (China) and is a commercial coating (KNC997).

Synthesis of VT

The synthesis of VT (Figure 1a) was conducted by dissolving 15.2 g (0.05 mol) of VAN in 150 mL DMF within a 500 mL three-necked flask equipped with a reflux condenser under continuous stirring. Following complete dissolution, 13.7 g (0.05 mol) of TA was introduced into the homogeneous solution, and the reaction was performed under a nitrogen atmosphere with heating to 90°C maintained for 6 hours. The resultant mixture was then cooled to ambient temperature, filtered to yield a yellow crude product, which underwent sequential triple washes with DMF and ethanol. Final purification was achieved by vacuum drying at 80°C for 12 hours, producing light yellow VT.

Synthesis of VTE

The synthesis of biobased epoxy (VTE) was conducted by sequentially introducing 27.13 g (0.1 mol) of VT, 185.0 g (2.0 mol) of epichlorohydrin, and 2.7 g (10 wt% relative to VT) of TBAB into a 500 mL three-necked flask equipped with a reflux condenser under nitrogen atmosphere. The mixture was heated to 80°C and maintained for 10 hours with continuous reflux. Subsequently, the temperature was reduced to 50°C, followed by slow addition of 20 g (0.2 mol) of 40% sodium hydroxide aqueous solution. The reaction proceeded at 50°C for an additional 6 hours before cooling to ambient temperature. The crude product underwent seven sequential water washes to eliminate by-products, followed by overnight drying with anhydrous sodium sulfate. Solvent removal was achieved by evaporation at 80°C for 2 hours, followed by vacuum drying at 80°C for 12 hours to ensure complete removal of residual epichlorohydrin, yielding the purified product.

Preparation of VTEC

The synthesis of VTEC involves a two-step reaction process: first, silica nanoparticles (2 parts), KH550 silane (25 parts), and silicone oil (50 parts) are homogeneously dispersed in ethyl

acetate and allowed to react for 12 hours at ambient temperature (28-30°C), followed by the controlled addition of VTE at a 1:2 molar ratio to KH550 for an 8-hour room-temperature reaction. The resulting solution is then applied onto aluminum or glass substrates via brush coating, spray deposition, or immersion techniques, with subsequent curing at ambient conditions for 48 hours to form a biobased hybrid epoxy coating featuring a robust cross-linked network structure. We respectively characterized the coating properties (transmittance, thickness and wettability) of the coatings obtained through three coating methods: brushing, spraying and dipping. As can be seen from the Fig. S19, using different coating methods will affect the thickness and transmittance of the coating. However, it has little effect on its wettability, such as the contact angle and the sliding angle. Considering aspects such as transparency, operational flexibility, the absence of the need for special equipment, and cost savings, the coatings obtained from our research were all applied by brush coating method.

Characterization

All coating characterizations were conducted on aluminum substrates, with the exception of the transmittance test performed on glass substrates and the dynamic icephobic performance evaluation carried out on carbon fiber composite material from the unmanned aerial vehicles.

The Fourier transform infrared (FT-IR) spectra of VT, VTE, and VTEC were recorded across the 4000-500 cm^{-1} range using a Nicolet 6700 spectrometer with a resolution of 4 cm^{-1} and 32 scan accumulations.

^{1}H nuclear magnetic resonance (^{1}H NMR) spectra were acquired in DMSO- d_6 solvent using a Bruker Avance III 600 MHz spectrometer, with chemical shifts referenced to residual solvent peaks.

The optical properties of the samples were investigated using an EV300 spectrophotometer, acquiring UV-vis absorption spectra across the 200-800 nm wavelength range.

Surface topography and roughness were evaluated through atomic force microscopy (AFM, MFP-3D) measurements.

The VTEC thickness was measured with a paint film-thickness gauge (Sanliang CT400, Japan).

The adhesive force between the VTEC and the substrate were evaluated by international standards of ISO 2409:2020 (cross-cut test).

Wettability was assessed by depositing 5 μL deionized (DI) water droplets on the coated surfaces and analyzing their static contact angles using a Kruss DSA 100 optical tensiometer. Notably, for investigating the effect of surface inclination on droplet sliding velocity, 10 μL droplets were employed. Moreover, the data obtained were all the average values calculated

from the results of 5 measurements. Specifically, for VTEC, five different samples were selected for measurement, and on the same sample, five locations were chosen for wetting property measurement, in order to ensure the accuracy and reliability of the results.

The anti-icing performance of the coatings was evaluated by measuring the icing delay time (IDT) through a controlled experimental setup. Each specimen was mounted on a thermoelectric cooling stage maintained at a constant surface temperature of -15°C, whereupon 15 μL deionized water droplets were deposited at controlled intervals using a precision micropipette system. The entire icing process was recorded in real-time using a camera. To ensure statistical reliability, five replicate tests were conducted for each sample, and the arithmetic mean of these measurements was adopted as the representative IDT value.

Deionized water was introduced into a polytetrafluoroethylene (PTFE) square mold (1.5 cm × 1.5 cm) positioned atop the test specimen, which was subsequently inverted and subjected to a 24-hour freezing period at -20°C in a controlled refrigeration unit. Following solidification, the ice sample was mechanically detached while a push-pull force gauge precisely measured the peak detachment force (F), with ice adhesion strength (τ_{ice}) determined through the established calculation methodology.

$$\tau_{ice} = \frac{F}{A} \tag{1}$$

The τ_{ice} measurements were systematically performed with a standardized contact area of 2.25 cm^2 between the test specimens and the ice surface, employing bare aluminum plates as baseline controls for comparative analysis with coated aluminum panels. A minimum of five independent tests were conducted for each sample configuration, and the reported values represent the arithmetic mean of these repeated measurements to ensure statistical reliability.

The chemical stability is mainly determined using three different solutions, namely HCl solution with pH=1, NaOH solution with pH=14, and NaCl solution with 3.5 wt%. Immerse the coating in the relevant solution, and take it out every week (for 7 days) to conduct the tests for contact angle and sliding angle.

The thermal cycling experiment involves conducting a high-low temperature cycling on the sample. First, the sample is placed at a low temperature (-20 ℃) for 1 hour. After 1 hour, it is then placed at a high temperature (80 ℃) for another 1 hour. This constitutes one cycle.

Electrochemical characterization was performed using a three-electrode configuration with a Princeton VersaStat 4 potentiostat, employing a 3.5 wt% NaCl aqueous solution as the electrolyte medium. The working electrode consisted of 1 cm^2 coated samples that were preconditioned in the solution for 60 minutes prior to testing, while Ag/AgCl and platinum

served as the reference and counter electrodes, respectively. All measurements were conducted under controlled environmental conditions to ensure experimental reproducibility.

Prior to experimentation, samples were sterilized in 10 mL centrifuge tubes at UV-light for 20 minutes. Three replicate 12 mL bacterial culture tubes were each filled with 3 mL of Luria-Bertani (LB) broth, inoculated with single colonies of Escherichia coli and Staphylococcus aureus from solid media, and incubated overnight at 37°C with shaking at 200 rpm. Following 15-hour cultivation, the bacterial suspension was centrifuged, washed with sterile water, and resuspended to achieve a final concentration of 10^8 CFU/mL. For bacterial adhesion testing, 150 μL of standardized bacterial suspension was applied to each sample surface in a 24-well plate, while control wells received only bacterial solution. After PBS elution, serial dilutions (10^{-3}) were prepared and plated onto LB agar. After 20-hour incubation at 37°C, colony-forming units (CFU) were enumerated within the 30-300 CFU range for accurate quantification.

Dynamic Icephobic Properties

The experimental investigation was conducted in Beihang University's specialized icing chamber, a 3m×3m×3.5m facility equipped to accommodate test models and measurement apparatus through its integrated mounting frame. Temperature regulation within the chamber spanned from ambient conditions down to -25°C with ±0.5°C precision, achieved while maintaining controlled humidity levels via coordinated operation of dehumidification and spray systems. Supercooled water droplets with median volume diameters (MVD) adjustable between 20-50 μm were generated using a pneumatic nozzle array calibrated via phase Doppler particle analyzer (PDPA), with flow rate modulation enabling precise control over liquid water content (LWC). A ducted fan system permitted independent adjustment of air velocity (0-20 m/s) and droplet impingement speed to simulate diverse atmospheric icing scenarios, including glaze and rime icing conditions. Real-time monitoring of temperature and relative humidity was performed using digital sensors, with the chamber's humidity regime dynamically controlled by balancing spray system output against dehumidification capacity to replicate specific environmental parameters. This comprehensive experimental setup enables systematic study of UAV icing phenomena across a broad spectrum of operational conditions.

The dynamic icing and anti-/de-icing processes were captured using a Phantom VEO 710L high-speed camera (7000 fps at 1280×800 resolution) equipped with a Canon 50mm lens, illuminated by two RPS Studio Light units (Models RS-5610 and RS-5620). Image analysis in MATLAB was employed to extract quantitative data from the recordings. Experiments utilized a DJI 9443 propeller (24 cm diameter, typical for civil multi-rotor UAVs) driven by a 2210-980KV brushless DC motor (12V DC power supply, 30V 10A power source) at 4000 rpm,

yielding Reynolds numbers of 32.4k, 46.2k, and 42.9k at 25%, 50%, and 75% spanwise positions respectively. Current fluctuations were monitored via Hall effect sensors. Test conditions simulated UAV hovering (0° pitch angle) with 10 m/s airflow delivering supercooled droplets (20 μm MVD, 2.0 g/m³ LWD) at -5°C ambient temperature, resulting in an advance ratio of 1.6. These parameters replicate operational icing scenarios for unmanned aerial vehicles.

Supplementary Figures

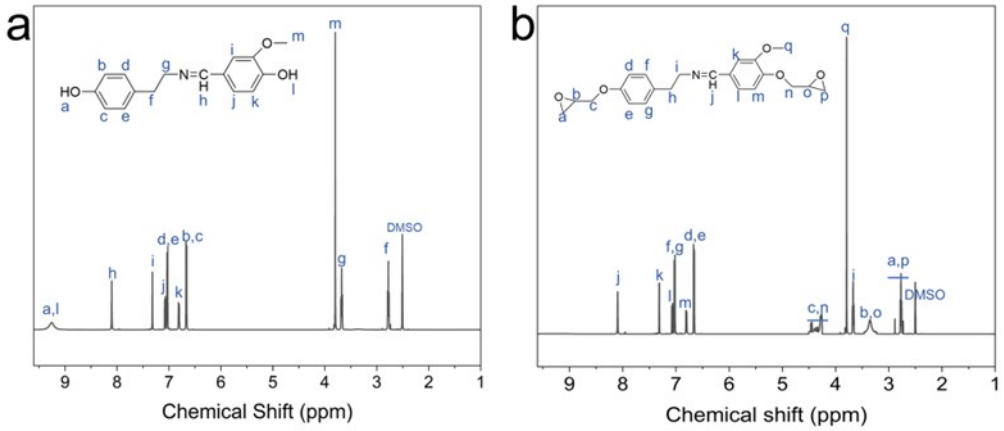

Fig. S1. ^{1}H NMR spectra of VT (a) and VTE (b)

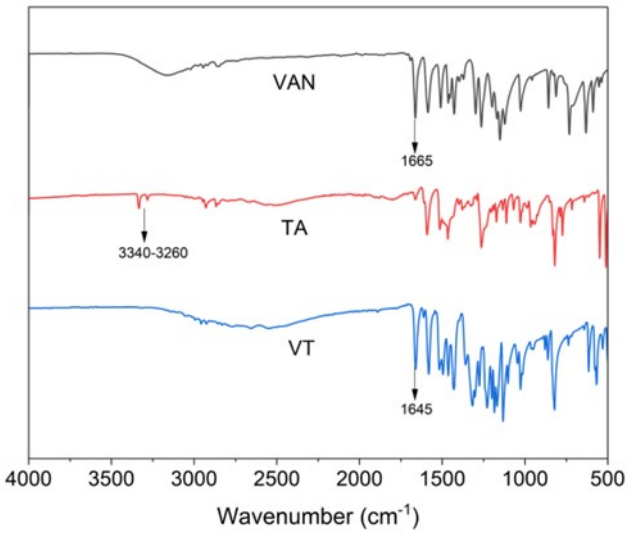

Fig. S2. FT-IR spectra of VAN, VT, and VT

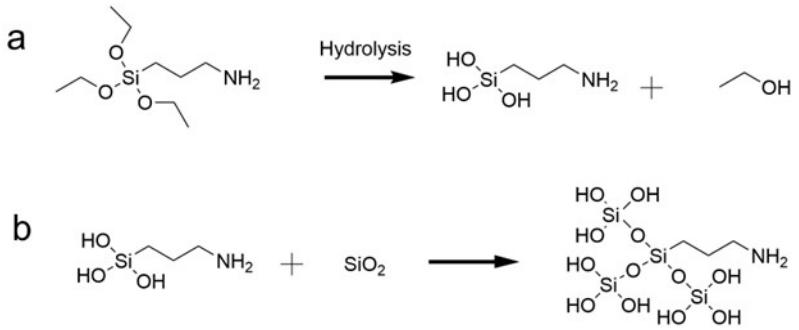

Fig. S3. Schematic of the synthesis mechanism of the functional SiO_2.

Fig. S4. The oil absorption process of oil absorbing paper on the coating surface.

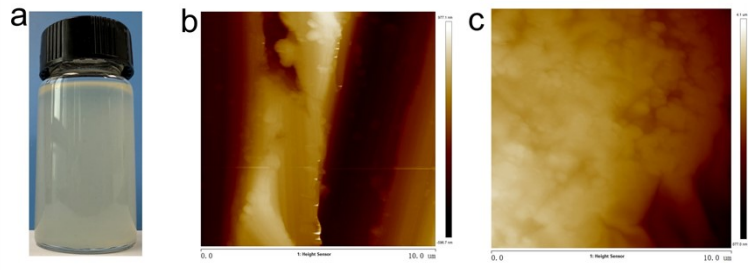

Fig. S5. (a) Image of coatings solution before curing. AFM Images of the (b) Al plate and (c) VTEC.

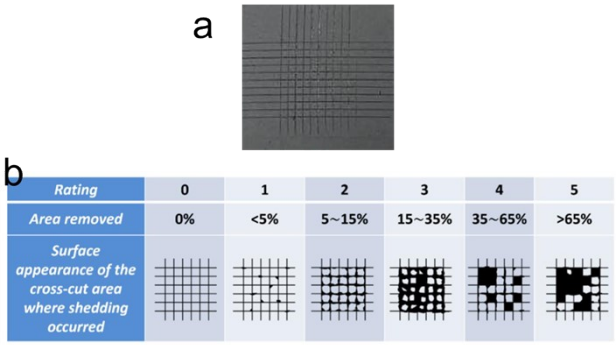

Fig. S6. (a) The Coating adhesion image, and (b) adhesion evaluation criteria in ISO 2409:2020.

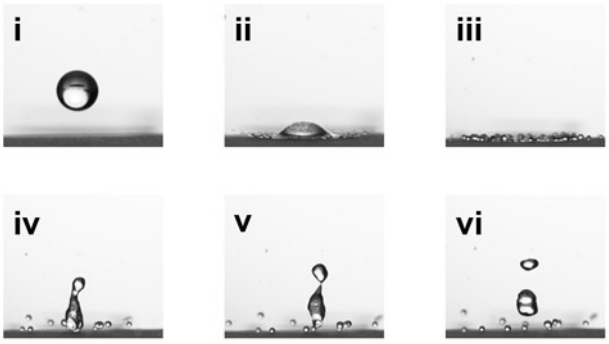

Fig. S7. A water droplet bouncing behaviors on the SHC surface.

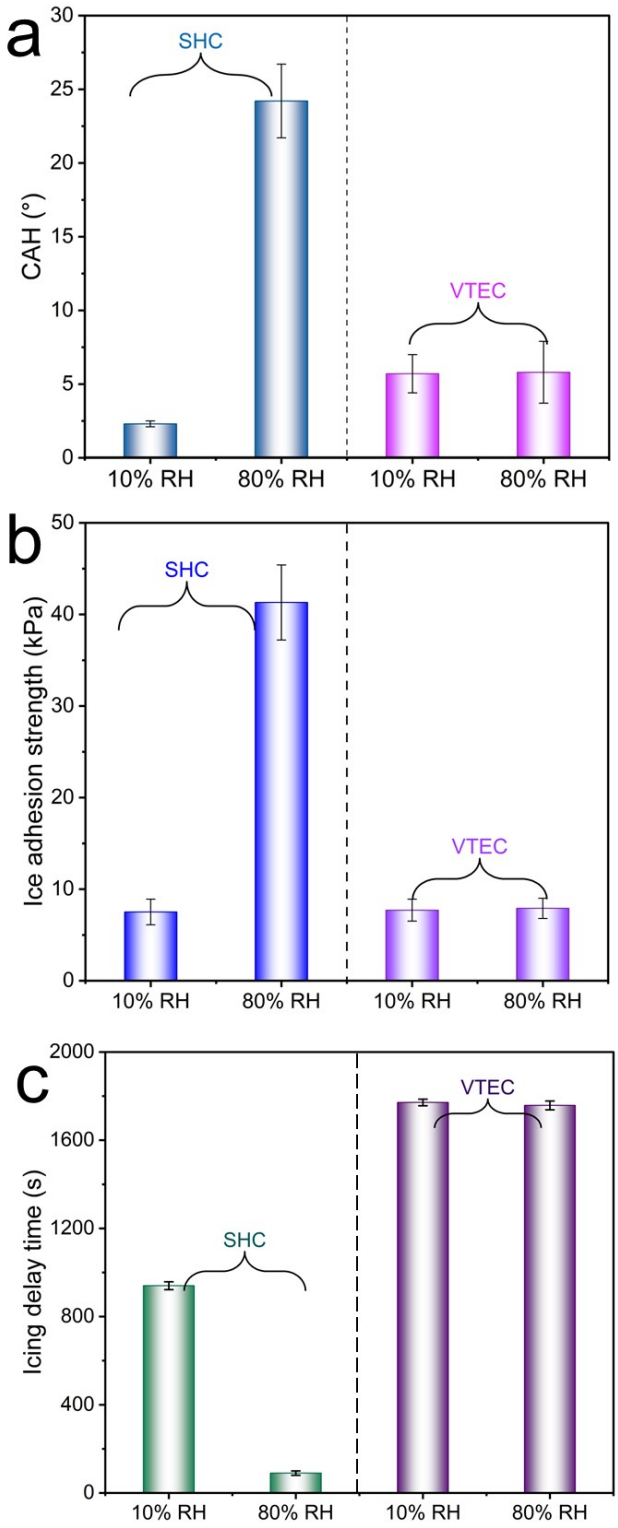

Fig S8. The CAH, ice adhesion strength and icing delay time of SHC and VTEC under different humidity conditions

Fig. S9. The icing delay process of SHC at -15 °C and 10% relative humidity.

Fig. S10. The icing process over uncoated propeller.

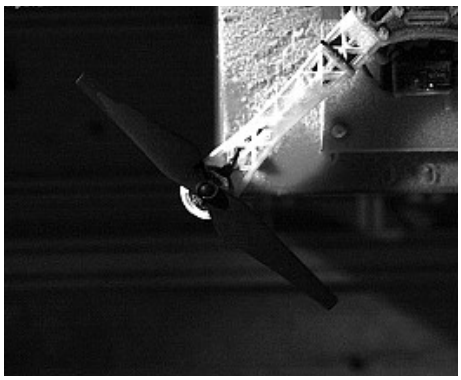

Fig. S11. The icing process over SHC-coated propeller.

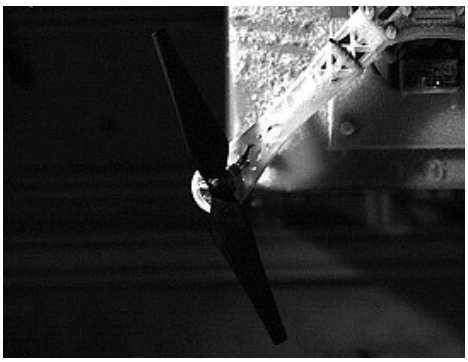

Fig. S12. The icing process over VTEC-coated propeller.

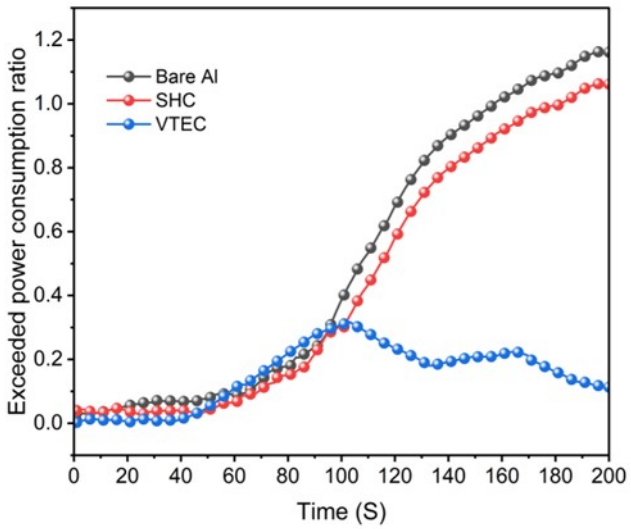

Fig. S13. Power consumption increasing ratio during 200s icing duration time.

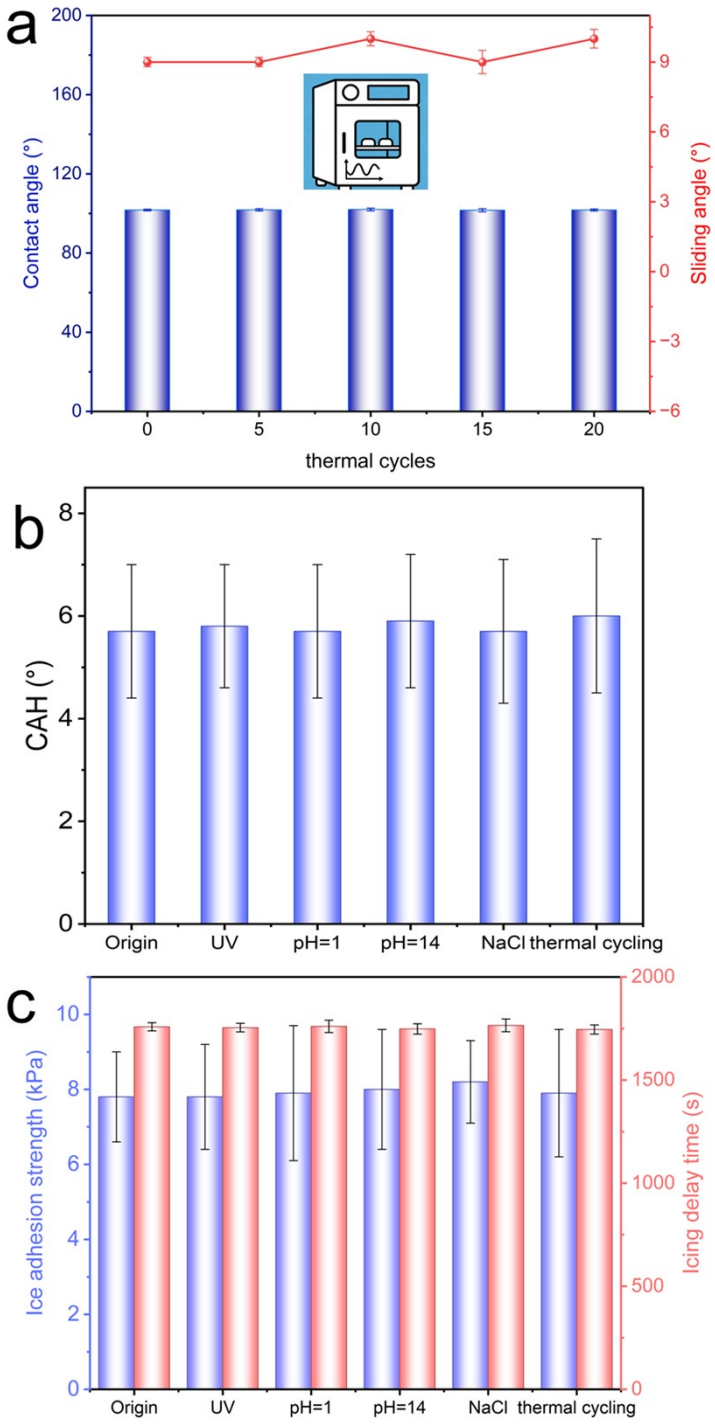

Fig. S14. The WCA and SA of VTEC under different heat cycle times, as well as the CAH, ice adhesion strength and ice formation delay time of VTEC after being treated under different conditions

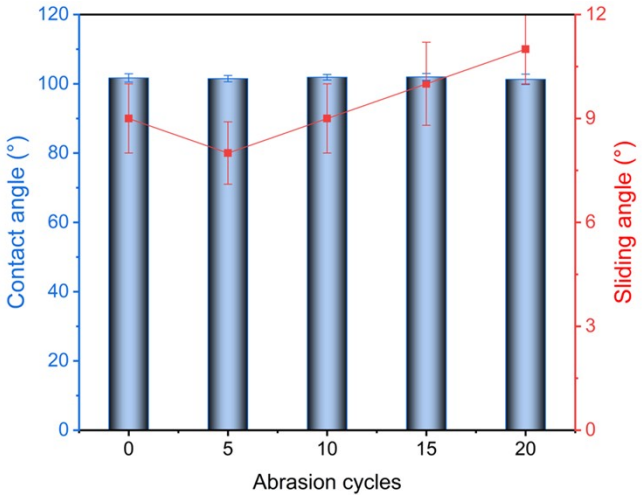

Fig. S15. The changes of WCA and SA with the increase in the number of abrasion cycles

After 20 cycles of application, the contact angle and sliding angle of the developed coating exhibited minimal variation, as illustrated in the accompanying figure. This observation underscores the coating's exceptional wear durability. The robust performance can be primarily ascribed to two key aspects: First, the inherently smooth surface profile reduces frictional forces during operation; Second, the cross-linked molecular architecture significantly bolstered the mechanical resilience of the coating. These findings have been incorporated into the updated supplementary materials for comprehensive reference.

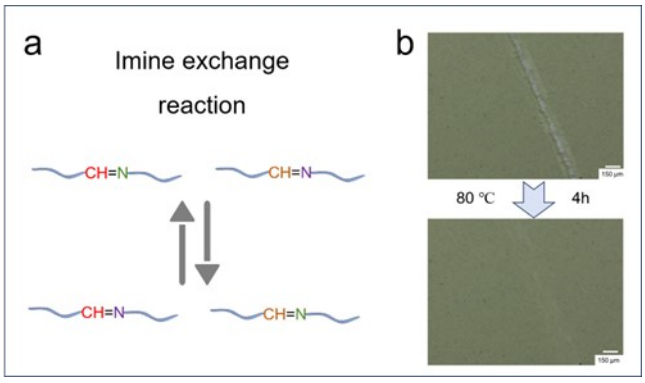

Fig. S16. (a) The mechanism of self-healing. (b) The optical images of VTEC self-healing under 80 ℃.

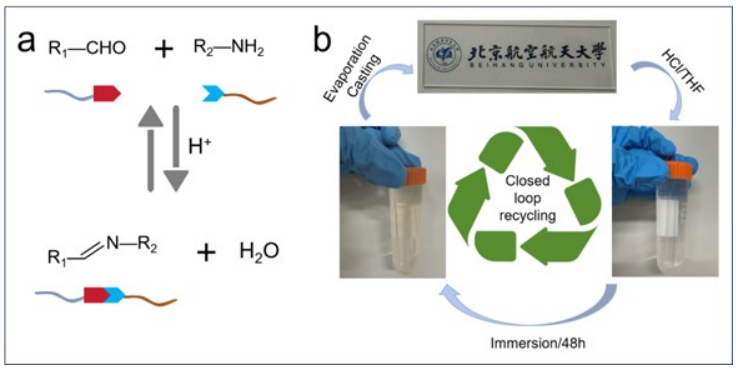

Fig. S17. (a) The mechanism of recycling. (b) The recycling process of VTEC.

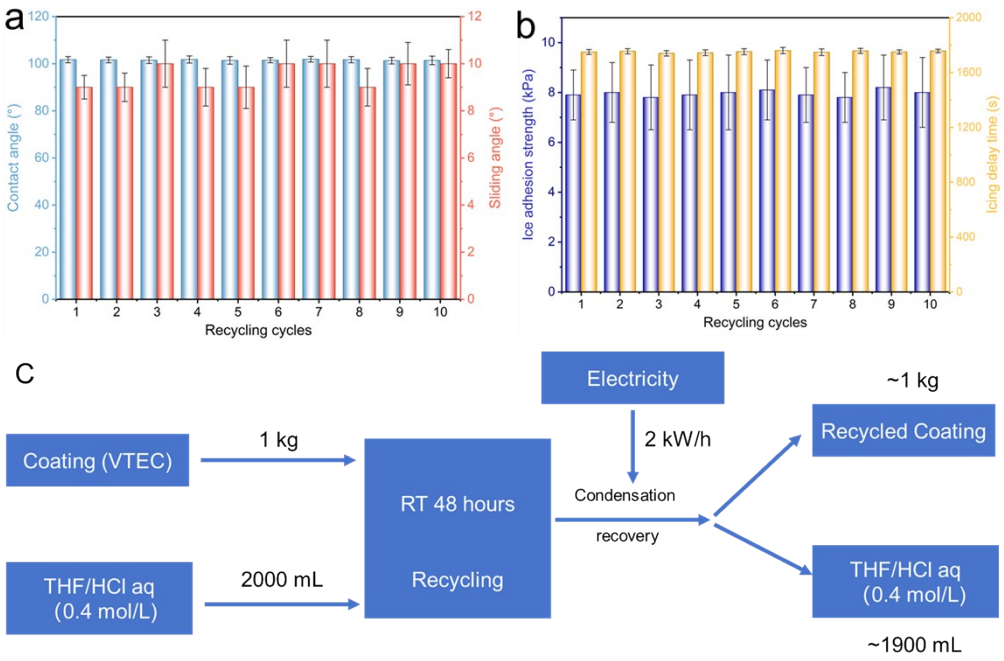

Fig. S18. The WCA, SA, ice adhesion strength and icing delay time of recycled coating under different recycling cycles. Flowcharts of the recycling process analyzed with LCA.

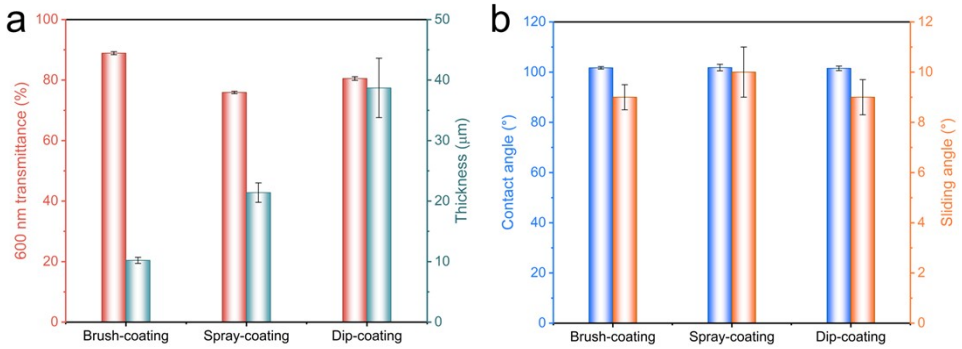

Fig. S19. (a) The transmittance and thickness under different coating methods, (b) the contact angle and sliding angle under different coating methods

Supplementary Table

Table S1 The compassion of icephobic performance of different dynamic icephobic coatings

ice adhesion strength (kPa)	icing delay time (s)	number of ice-shedding	EPC	Ref.
8.2	857	2	0.21	[1]
8.1	833	2	0.14	[2]
7.8	1758	2	0.11	This work

References

1 X. Wang, X. Huang, L. Tian, Z. Ji, H. Sheng, S. Xu, X. Li, H. Liu, *Adv. Funct. Mater.,* 2025, **35**, 2415952. https://doi.org/10.1002/adfm.202415952.

2 X. Wang, X. Huang, Z. Ji, L. Tian, H. Sheng, S. Xu, H. Liu, *Compos. Part B,* 2026, **311**, 113249. https://doi.org/10.1016/j.compositesb.2025.113249.

Supplementary Movies

Video S1. The oil-test paper was still dry and clean on the VTEC.

Video S2. A 10 μL water droplet slides fluently on the VTEC with a tilting angle of 20°..

Video S3. The non-sticking performance of the VTEC to the double-sided tape.

Video S4. The non-sticking performance of the VTEC to the Electrical tape.

Video S5. The self-cleaning performance test of the VTEC by immersing the VTEC into various liquids, such as acid, alkali, salt, tea, and cola. After taking out the VTEC, there was no residue of these liquids on the VTEC.

Video S6. The self-cleaning performance test of the VTEC by removing the solid pollutants with the mimic raindrops.

Video S7. The VTEC's wind-aided de-icing test. Due to the tremendous shear strength of the SHC and the bare Al plate, the ice block stuck firmly to these surfaces, whereas the ice block on the VTEC blew away as soon as it came into contact with compressed air.

Video S8. The icing process of bare Al under -15 ℃ and 80% relative humidity.

Video S9. The icing process of SHC under -15 ℃ and 80% relative humidity.

Video S10. The icing process of HVIC under -15 ℃ and 80% relative humidity.

Video S11. The icing process of SHC under -15 ℃ and 10% relative humidity.